



Brief communication: Firn data compilation reveals the evolution of the firn air content on the Greenland ice sheet

Baptiste Vandecrux^{1,2}, Michael MacFerrin³, Horst Machguth^{4, 5}, William T. Colgan¹, Dirk van As¹, Achim Heilig⁶, C. Max Stevens⁷, Charalampos Charalampidis⁸, Robert S. Fausto¹, Elizabeth M. Morris⁹, Ellen Mosley-Thompson¹⁰, Lora Koenig¹¹, Lynn N. Montgomery¹¹, Clément Miège¹², Sebastian B. Simonsen¹³, Thomas Ingeman-Nielsen², Jason E. Box¹

¹ Geological Survey of Denmark and Greenland, Copenhagen, Denmark.

² Department of Civil Engineering, Technical University of Denmark, Lyngby, Denmark.

10 ³ Cooperative Institute for Research in Environmental Sciences, University of Colorado, Boulder, CO USA

⁴ Department of Geosciences, University of Fribourg, Fribourg, Switzerland

⁵ Department of Geography, University of Zurich, Zurich, Switzerland

⁶ Department of Earth and Environmental Sciences, LMU, Munich, Germany

⁷ Department of Earth and Space Sciences, University of Washington, WA USA

15 ⁸ Bavarian Academy of Sciences and Humanities, Munich, Germany

⁹ Scott Polar Research Institute, Cambridge University, United Kingdom

¹⁰ Byrd Polar and Climate Research Center and Department of Geography, Ohio State University, Columbus, OH USA.

¹¹ National Snow and Ice Data Center, University of Colorado, Boulder, NV, United States

¹² Department of Geography, Rutgers University, Piscataway, NJ, United States

20 ¹³ National Space Institute, Technical University of Denmark, Kgs. Lyngby, Denmark

Correspondence to: B. Vandecrux (bava@byg.dtu .dk)

Abstract. The firn covering the Greenland ice sheet interior can retain part of the surface melt, buffering the ice sheet's contribution to sea level, but its characteristics are still little known. Using remote-sensing observations from 2000- 2017, we estimate that firn covers $1,405,500 \pm 17,250 \text{ km}^2$ of the ice sheet. We present 344 firn-core-derived observations of the top 10 m firn air content (FAC₁₀), indicative of the firn's meltwater retention capacity. FAC₁₀ remained stable in the coldest 74% of the firn area during 1953-2017, while FAC₁₀ decreased in the warmest and driest 12% of the firn area between 1997-2008 and 2011-2017, resulting in a loss of $180 \pm 78 \text{ km}^3$ ($-26 \pm 11\%$) of air from the near-surface firn.

30 1. Introduction

More than half of the Greenland ice sheet's current contribution to sea level rise stems from surface melt and subsequent runoff (van den Broeke et al., 2016). During summer, surface melt occurs across a large area of the ice sheet, even reaching the highest ice sheet elevations during extremely warm summers like 2012 (Nghiem et al., 2012). Most of the surface meltwater produced in the firn-covered interior of the ice sheet is refrozen into the snow and firn and does not immediately contribute to sea-level rise (Harper et al., 2012). This retention capacity of the firn is controlled by (i) the areal extent of the firn; (ii) the firn air content (FAC); (iii) firn temperature; and (iv) firn permeability. In this study, we use in-situ and remotely-sensed observations to estimate the firn's extent and its air content in the upper 10 m.



The first attempt to delineate the ice-sheet firn area into characteristic zones dates back to the 1950s (Benson, 1962). Later studies delineated the firn area using satellite remote sensing (e.g. Nolin and Payne, 2007) but had limited spatial and temporal coverage. Recently Fausto et al. (2018) published maps of remotely-sensed end-of-summer snowline but did not discuss the simple implication of these snowlines for the firn area extent.

5 The FAC is the volume of air contained in the firn from the surface to a certain depth per unit area. It indicates for that depth range the maximum volume available to store percolating meltwater either in liquid or refrozen form (Harper et al., 2012). Harper et al., (2012) used two years (2007 and 2008) of observations from 15 sites along the western slope of the ice sheet to estimate the spatially integrated FAC of the entire percolation area in spite of the diversity of firn structures across the ice sheet (Forster et al. 2014; Machguth et al., 2016). Estimation of the FAC was also made using firn models forced by
10 regional-climate-model (RCM) output (e.g. Ligtenberg et al., 2018) but model results differ significantly from each other in terms of firn density and therefore of FAC (Steger et al., 2016).

The depth to which meltwater may percolate, and therefore to which FAC must be calculated, varies with melt intensity and firn permeability. Heilig et al. (2018) did not observe percolation deeper than 2.3 m below the surface at 2300 m a.s.l. in west Greenland indicating that, at their study site, only the near-surface FAC was being used to store meltwater. In a warmer
15 region, ~400 km to the north and at 1555 m a.s.l., Humphrey et al. (2012) observed percolation below 10 m meaning that the FAC of the whole firn column, from the surface to pore-close-off depth, might be used for meltwater retention. Nevertheless, Machguth et al. (2016) showed that percolation depth may not increase linearly with melt intensity and that refrozen meltwater can reduce percolation, subsequently preventing meltwater from accessing part of the FAC. Due to the absence of an ice-sheet-wide estimation of percolation depth and to the scarcity of firn observations covering the whole firn column, we
20 here focus on the top 10 m of firn, for which numerous observations cores are available, and assume that the firn air content in these top 10 m (FAC_{10}) represents the maximum volume of meltwater that can be stored in the firn.

In this study, we first estimate the firn area extent using remotely-sensed end-of-summer snow extent maps from Fausto et al., (2018). We then calculate the FAC_{10} using a set of 344 firn cores collected between 1953 and 2017. We finally present the spatial distribution and where possible the temporal evolution of FAC_{10} .

25 2. Data and methods

2.1. Firn area extent

Fausto et al. (2018) used surface radiance remotely sensed by the MODIS Terra satellite between 2000 and 2017 along with in-situ measurements of albedo at PROMICE automatic weather stations (Ahlstrøm et al., 2008) to estimate the end-of-summer snow-covered and bare ice areas. Using these data, we determine the firn area, defined as the region where only
30 snow has been detected during the entire 2000-2017 period.



2.2. Firn cores dataset

We gathered from the literature 324 firn-density profiles from cores that were at least 5 m long (Table 1 and S1 of the Supplementary Material) supplemented by 20 firn cores extracted in April-May 2016 and 2017 as part of the FirnCover campaigns and for which the density was measured at 10 cm resolution. Potential gaps in the density profile were filled using a logarithmic function of depth fitted to the available densities. When near-surface snow densities were missing, we assigned a density of 315 kg/m³ (Fausto et al., 2018) to the top centimetre of snow before the gap-filling.

2.3. Calculation of the FAC₁₀

For a discrete density profile, the FAC₁₀ in m³ m⁻² is calculated to depth z_N as:

$$FAC_{z_N} = \sum_{k=1}^N m_k (1/\rho_k - 1/\rho_{ice}) \quad [1]$$

where, for each section k , ρ_k is the density and m_k is the mass. The density of the ice formed after meltwater infiltration and refreezing, ρ_{ice} , is set to 873 kg m⁻³ after Machguth et al. (2016). The value for ρ_{ice} was seen to vary within ± 25 kg m⁻³ by Machguth et al., 2016 and Harper et al., 2012 used a value of 843 kg m⁻³. Changing ρ_{ice} by ± 25 kg m⁻³ leads to a variation of ± 1 to 10% for FAC₁₀ values ranging from 5 to 1 m³ m⁻². Addressing the variability of ρ_{ice} and its potential drivers is beyond the scope of this study.

With 121 cores shorter than 10 m in our dataset, we need to extrapolate shallow measurements to a depth of 10 m. For that we find the 10+ m core that best matches the FAC vs. depth profile of the shallow core, with lowest Root Mean Squared Difference (RMSD) amongst all available cores, and append the bottom section of this ‘twin’ core to the FAC profile of the shallow core (see Figure S1 of the Supplementary Material). When testing this methodology on the available 10+ m long cores from which we remove the deepest 3 m of the FAC profile, find a mean difference between extrapolated and real FAC₁₀ inferior to 1% and a RMSD of 3-15% for FAC₁₀ values ranging from 5 to 1 m³ m⁻².

The accuracy of the firn and infiltration ice densities as well as the effect of spatial heterogeneity can be assessed by comparing FAC₁₀ measurements located within 1 km (Figure S2 of the Supplementary Material). The standard deviation of co-located FAC₁₀ observations is below 0.15 m³ m⁻² for the majority of sites (20 of 27). We therefore attach to any FAC₁₀ measurement an uncertainty of ± 0.3 m³ m⁻², twice the standard deviation, ± 6 to 30% for FAC₁₀ values ranging from 5 to 1 m³ m⁻².

2.4. Zonation of the firn air content

FAC₁₀ depends on the site’s temperature and accumulation history and on meltwater refreezing at depth (Reeh, 2008). We extract each core site’s long-term (1970-2014) average net snow accumulation \bar{b} and long-term (1970-2014) average air



temperature \bar{T}_a respectively from Box (2013) and Box et al. (2013) (Figure 1a). We also find \bar{b} and \bar{T}_a for all locations that occur within the firn area derived in this study (outlined area in Figure 1b).

Borrowing the terminology from Benson (1962), we define three regions where FAC_{10} shows markedly different behaviours: (1) the Dry Snow Area (DSA, amber area in Figure 1a); (2) the Low Accumulation Wet Snow Area (LAWSA, red area in Figure 1a); (3) the High Accumulation Wet Snow Area (HAWSA, green area in Figure 1a). The DSA encompasses low temperature regions of high altitude or latitude where melt is rare and where FAC_{10} can be explained by well-known dry-firn compaction equations dependent on \bar{b} and \bar{T}_a (amber area in Figure 1a). Toward higher \bar{T}_a (lower altitude and/or latitude) two patterns are evident. At lower \bar{b} sites in the LAWSA, more scatter appears in FAC_{10} , and a slope change occurs in the FAC_{10} 's temperature dependency (Figure 1c). At higher \bar{b} (in the HAWSA), FAC_{10} remains higher than at locations with similar \bar{T}_a in the LAWSA and the slope of the temperature dependency is different from the one found in the DSA or LAWSA (green area in Figure 1d).

The boundary between the colder (DSA) and warmer regions (LAWSA and HAWSA) can be defined as the \bar{T}_a where the dry firn densification cannot explain FAC_{10} variations and increasing scatter appears in the FAC_{10} values (Figure 1c). We set this threshold to $\bar{T}_a = -16^\circ\text{C}$ as it is the temperature for which the standard deviation of FAC_{10} within 1°C -wide bins first exceeds $0.3 \text{ m}^3 \text{ m}^{-2}$ (Figure 1c). Few firn cores are available in the transition zone from LAWSA to HAWSA and a boundary could be anywhere between 543 mm w.eq./yr (core with highest accumulation in the LAWSA, Figure 1a) and $762 \text{ mm w.eq. yr}^{-1}$ (core with lowest accumulation in HAWSA, Figure 1a). We chose the rounded value of $600 \text{ mm w.eq. yr}^{-1}$ to separate LAWSA from HAWSA. The geographical delineations of the DSA, LAWSA and HAWSA are presented in Figure 1a.

2.5. Firn air content mapping

To map FAC_{10} over the entire firn area from our collection of observations, we fit empirical functions of \bar{b} and \bar{T}_a to FAC_{10} measurements and use these functions to predict FAC_{10} anywhere in the firn area. We prefer this empirical approach to purely statistical approaches (e.g. kriging) or to the use of RCM and firn models which still do not accurately reproduce observations of firn densities and thus FAC_{10} in the lower accumulation area (Steger et al., 2016; Langen et al., 2017). The form of these empirical functions is arbitrary but is tightly constrained by the numerous FAC_{10} observations that they should fit. In this section, we briefly explain how we build these functions while further details and illustrations are available in Figure S3 of the Supplementary Material.

2.5.1. Dry Snow Area

In the DSA, we use the steady-state firn densification model by Arthern et al. (2010) and we tune the surface snow density to 302 kg m^{-3} through least squares method to match the 209 available FAC_{10} observations (Figure S3 in the Supplementary



Material). We also investigated other densification laws and the one from Arthern et al. (2010) gave the best match with FAC_{10} observations.

2.5.2. Low Accumulation Wet Snow Area

FAC_{10} observations in the LAWSA are correlated with \bar{b} and anti-correlated with \bar{T}_a (Figure S3 in Supplementary Material). We therefore constrain the form of our empirical function $\widehat{FAC}_{10}(\bar{b}, \bar{T}_a)$ to the sum of an increasing linear function of \bar{b} and a decreasing piecewise-linear function of \bar{T}_a . There are an insufficient number of observations to resolve the FAC_{10} distribution each year, so we group measurements from different years until there are enough points in each group to constrain our empirical function. We therefore group 10 observations from 1997-1998 (having good spatial coverage but limited number of cores) with 35 measurements from 2005-2008 (numerous but geographically concentrated) and fit a function $\widehat{FAC}_{10_{1998-2008}}(\bar{b}, \bar{T}_a)$ to them. We also group 35 FAC_{10} observations from 2011-2017 to which we fit a function $\widehat{FAC}_{10_{2011-2017}}(\bar{b}, \bar{T}_a)$. To allow a smooth transition between these empirical functions used in the LAWSA and the one used in the DSA, we also include in the fitting process the FAC_{10} observations available in the lower DSA where $-17^\circ\text{C} \leq \bar{T}_a < -16^\circ\text{C}$.

We investigate the robustness of our method using a sensitivity analysis for each period separately. For 1000 repetitions, we randomly exclude four observations (respectively 9% and 11% of the observations in 1997-2008 and 2011-2017) and fit our empirical function $\widehat{FAC}_{10}(\bar{b}, \bar{T}_a)$ to the remaining measurements. We then calculate the standard deviation of all possible \widehat{FAC}_{10} at each (\bar{b}, \bar{T}_a) location and double it to quantify the 95% envelope of uncertainty that applies to any predicted FAC_{10} in the LAWSA depending on (\bar{b}, \bar{T}_a) . Since we do not consider that prediction can be more precise than field measurements, we set $0.3 \text{ m}^3 \text{ m}^{-2}$ as the minimum possible uncertainty.

2.5.3. High Accumulation Wet Snow Area

The HAWSA is described by only 15 firn cores drilled between 2010 and 2017 at 7 sites in the interior of the HAWSA, more than 20 km from the firn line. To overcome the scarcity of observations we use our remotely-sensed firn line as additional measurements where $FAC_{10} = 0 \text{ m}^3 \text{ m}^{-2}$. We then fit our empirical function $\widehat{FAC}_{10}(\bar{b}, \bar{T}_a)$ as follows. In the surroundings of the core sites, we use a linear function of \bar{T}_a fitted through least squares to the FAC_{10} observations: $\widehat{FAC}_{10}(\bar{T}_a) = -0.07 * \bar{T}_a + 3.4$ (RMSD = $0.25 \text{ m}^3 \text{ m}^{-2}$, Figure S3 in the Supplementary Material). The residuals of this fit did not show any correlation with \bar{b} meaning that not enough measurements are available to disentangle the control of \bar{b} and \bar{T}_a on FAC_{10} in the HAWSA. We then need to describe how the FAC_{10} decreases from the core sites down to $0 \text{ m}^3 \text{ m}^{-2}$ at the remotely-sensed firn line. We can make three estimates: i) a mid-range estimate where FAC_{10} is bilinearly interpolated between the available firn cores and the firn line; ii) an upper-range estimate where FAC_{10} follows the temperature dependency presented



above until the firn line where it drops abruptly to $0 \text{ m}^3 \text{ m}^{-2}$; and iii) a lower-range estimate where the FAC_{10} drops to $0 \text{ m}^3 \text{ m}^{-2}$ shortly after the observations. These three surfaces are presented in more detail in Figure S3 in the Supplementary Material. The mid-range estimate is considered as our most realistic estimation and is the empirical function $\widehat{\text{FAC}}_{10}(\bar{b}, \bar{T}_a)$ we use for the mapping of FAC_{10} in the HAWSA while half the spread between the upper- and lower-range estimates quantifies the uncertainty applying to our FAC_{10} map.

3. Results and Discussion

3.1. Delineation of the firn area

The firn area, illustrated in Figure 1b, covers at least an area of $1,405,500 \text{ km}^2$ or 78.5 % of the ice sheet (when compared to the contiguous ice extent from Citterio and Ahlstrøm (2013)). Moving the firn line 1 km in- or outwards (the resolution of the MODIS surface radiance product) suggest an uncertainty of $\pm 17,250 \text{ km}^2$ (~1%). However, one should keep in mind that the firn line is an idealized view of a patchy and gradual transition from bare ice to snow and firn that survived the summer melt in previous years (Benson, 1962). Spatial heterogeneity in melt and snowfall leave isolated snow and firn patches at the end of the melt season which might be missed by the method of Fausto et al. (2018). Using the average from 18 years of data gives a robust firn line and reduces the noise from local heterogeneities but also provides the absolute minimum extent of the firn area during 2000-2017. Ephemeral or thinner firn patches may exist outside of our strict delineation but we do not believe they play an important role in the overall retention capacity of the firn.

3.2. Stable FAC_{10} in the Dry Snow Area

The spatial distribution of FAC_{10} in the DSA is shown in Figure 2. In that region representing 74% of the firn area, we find a spatiotemporally average FAC_{10} value of $4.9 \text{ m}^3 \text{ m}^{-2}$. We find a RMSD between predicted and observed FAC_{10} of $0.2 \text{ m}^3 \text{ m}^{-2}$ (Figure S3 in the Supplementary Material). Assuming a normal distribution of errors, 95% of all FAC_{10} observations in the DSA are within an uncertainty range of $\pm 0.4 \text{ m}^3 \text{ m}^{-2}$ (twice the RMSD) of the predicted one. We consider the absence of temporal trend in the deviation between measured and predicted FAC_{10} as evidence of the stability of the FAC_{10} in the DSA between 1953 and 2017. When integrating FAC_{10} over the extent of the DSA and considering an uncertainty of $\pm 0.4 \text{ m}^3 \text{ m}^{-2}$, we calculate that $5200 \pm 452 \text{ km}^3$ of air is contained within the top 10 m of firn.

3.3. Decreasing FAC_{10} in the Low Accumulation Wet Snow Area



For the LAWSA, comprising 12 % of the firn area, we find an average FAC₁₀ value of 4.3 m³ m⁻² for the 1997-2008 period. The estimated average FAC₁₀ for the 2011-2017 period is 3.3 m³ m⁻², 23% lower than for 1997-2008. The result of the sensitivity analysis (Figures 3b and 3c), confirms that the decrease in FAC₁₀ between the 1997-2008 and 2011-2017 is greater than the uncertainty associated to the two FAC₁₀ maps. The FAC₁₀ loss in the LAWSA is concentrated in a 60 km wide band above the firn line (Figure 2). Summing the FAC₁₀ and its uncertainty indicates that 690 ±50 km³ of air is contained within the LAWSA in 1997-2008 and 520 ±60 km³ in 2011-2017. This loss of 180 ±78 km³ of air content, 26 ±11% of the 1997-2008 air content in the LAWSA represents, if we assume that all the air content can be used to store meltwater, 150 ± 68 Gt (0.4± 0.2 mm sea level equivalent) of storage capacity available in 1997-2008 that had become unavailable by 2011-2017.

Recent studies attributed the increasing near-surface firn densities and subsequent loss of FAC to increasing surface melt and meltwater refreezing (de la Peña et al., 2015; Machguth et al., 2016; Graeter et al., 2018; Charalampidis et al., 2015). However, firn density and FAC are also greatly dependant on annual snowfall (Herron and Langway, 1980) and a decrease in snowfall could also trigger a decrease in FAC₁₀. Nevertheless, the lack of distributed observation of snow accumulation for the 1997-2017 period and the contradicting trends in precipitation given by the RCMs (Lucas-Picher et al., 2012; van den Broeke et al., 2016; Fettweis et al., 2017) make it impossible to quantify the contribution of snowfall into change in FAC₁₀. In our regional approach, we grouped measurements from different years, which made it impossible to define the precise years that were responsible for this loss of FAC₁₀. However, repeated observations in western Greenland (Machguth et al., 2016; Charalampidis et al., 2015) indicate that 2010 and 2012 extreme melt seasons are responsible for the greatest changes in near-surface firn density and FAC₁₀ during the 1997-2017 period.

Finally, the loss of FAC₁₀ near the firn line likely turned firn areas into bare ice and triggered the upward migration of the firn line. Unfortunately the relative uncertainty of our FAC₁₀ maps is greatest near the firn line (Figure 2 and 3) making it difficult to infer firn line migration from FAC₁₀ changes. Using our remotely-sensed firn line for all periods was a simplification but discussing its temporal evolution requires additional data and is beyond the scope of this study.

3.4. Potential deep meltwater percolation in the High Accumulation Wet Snow Area

In the HAWSA, comprising 14 % of the firn area, we calculate an average FAC₁₀ value of 2.4 m³ m⁻². The spatial distribution of FAC₁₀ is shown in Figure 2 while our estimated uncertainty map is presented in Figure 3. Summing over the HAWSA, we calculate that 560 ±154 km³ of air exists within the top 10 m of firn.

The markedly (up to 90%) higher FAC₁₀ in the HAWSA compared to the LAWSA for any given \bar{T}_a (Figure 1) indicates that for similar surface melt (of which \bar{T}_a is a proxy) the firn in the HAWSA was less dense and potentially less saturated by ice than in the LAWSA. In line with observations at aquifer sites located in the HAWSA (Forster et al., 2014), we hypothesize that in this region meltwater percolation may exceed 10 m, facilitated by high snow accumulation insulating the firn from the



winter cold. This deep percolation also implies that FAC_{10} may not be the most adequate indicator of the firm's retention capacity in the HAWSA as additional retention may occur at deeper than 10 m. The fate of this deep meltwater whether it refreezes below 10 m, flows to the nearest aquifer, or reaches the bed, remains unknown and requires further investigation.

3.5. Total firm meltwater storage capacity

5 The total air content in the DSA during 1953-2017, in the LAWSA during 2011-2017 and in the HAWSA during 2010-2017 can potentially accommodate $5,480 \pm 420$ Gt of meltwater (15 ± 1.2 mm sea level equivalent). Harper et al. (2012) estimated that the firm located in the long-term percolation area (as modelled by a RCM) could potentially store between 322 ± 44 Gt (when considering the top 10 m of firm) and $1\,289^{+388}_{-252}$ Gt (if considering the FAC to pore close-off depth). The smaller retention capacity found by Harper et al. (2012) mainly owes to the smaller area considered in their study. With our distributed approach, it is now possible to determine each year which areas of the firm are available to store meltwater and the available FAC_{10} given the extent of surface melt.

3.6. Uncertainty of long-term average climatic conditions

To investigate how uncertainties in \bar{b} and \bar{T}_a impacts our FAC_{10} maps, we repeat our procedure using the 1979-2014 \bar{b} and \bar{T}_a predicted by the Modèle Atmosphérique Régional (MAR; Fettweis et al., 2017), as illustrated in Figures S4 to S7 of the Supplementary Material. The MAR-derived FAC_{10} fits equally well (within measurements uncertainty, $RMSD < 0.03 \text{ m}^3 \text{ m}^{-2}$) the FAC_{10} observations. Since Box et al. (2013) gives 2 m air temperature and MAR gives surface temperature the value of \bar{T}_a threshold between DSA and LAWSA/HAWSA is adjusted to -20°C . Nonetheless differences between the two FAC_{10} predictions exist in areas where the spatial pattern of temperature and accumulation in Box (2013) and MAR differ, especially in the southern and eastern firm area. In these regions fewer cores are available to constrain the FAC_{10} estimates. More observations in these sparsely observed regions would therefore not only improve FAC_{10} estimates, but also elucidate which \bar{b} and \bar{T}_a source best describes the spatial pattern in FAC_{10} .

3.7. Isolated FAC_{10} measurements

In the LAWSA and HAWSA, our dataset also contains 40 firm cores that were too isolated in space and time to be used FAC_{10} in mapping. Isolated measurements nevertheless provide insight on how the FAC_{10} might have been at a given place and time. Renaud (1959) reported a measurement in the LAWSA with a FAC_{10} ~30% higher ($+ 1 \text{ m}^3 \text{ m}^{-2}$) than the one measured in 2006-2007. Conclusions from a single measurement are dubious, but it still indicates that the FAC_{10} may have



been significantly higher in the 1950's. Ten observations in the LAWSA in the 1980's by van der Veen, et al. (2001), did not appear systematically different than our calculated FAC_{10} for the 1997-2008 period, suggesting that FAC_{10} was similar in the LAWSA during these two periods. A last measurement raises questions in the HAWSA: the core 6348 by Mosley-Thompson et al. (2001) drilled in 1998 indicates a FAC_{10} of $3.9 \text{ m}^3 \text{ m}^{-2}$. It is a factor of 2.2 higher than our mid-range FAC_{10} estimate based on measurements from 2010-2017 and indicates either a drastic decrease in FAC_{10} between 1998 and 2010-2017 or inaccuracies of our methodology for that location. A re-survey of that location would be of great interest even though the 1998 core, being a single point in space, can always be suspected to be anomalous or not representative.

4. Conclusions

Our study provides, for the first time, a delineation of the firn area of the Greenland ice sheet over the 2000 – 2017 period. Using remote-sensing observations from 2000 to 2017, we estimate that firn covers $1,405,500 \pm 17,250 \text{ km}^2$ or 78.5% of the ice sheet. This result allows further study of possible migration of this boundary in the past or in the future. Additionally, we present a collection of 344 firn cores spanning 65 years from which the firn air content from the surface to 10 m depth (FAC_{10}) could be calculated. We identify three regions on the firn area in which FAC_{10} where we could fit empirical functions of long-term accumulation and temperature averages (\bar{b} and \bar{T}_a) to FAC_{10} measurements and explain the spatio-temporal evolution of FAC_{10} . The stability of the FAC_{10} in the Dry Snow Area (where $\bar{T}_a \leq -16^\circ\text{C}$) over the 1953-2017 period contrasts with a 21% decrease of FAC_{10} in the Low Accumulation Wet Snow Area (where $\bar{T}_a > -16^\circ\text{C}$ and $\bar{b} \leq 600 \text{ mm w.eq. yr}^{-1}$) between 1998-2008 and 2011-2017. This decreasing FAC_{10} translates into the loss of $168 \pm 138 \text{ Gt}$ ($0.5 \pm 0.4 \text{ mm}$ sea level equivalent) of meltwater retention capacity 1998-2008 and 2011-2017. In the High Accumulation Wet Snow Area (where $\bar{T}_a \geq -16^\circ\text{C}$ and $\bar{b} < 600 \text{ mm w.eq. yr}^{-1}$) we find an average FAC_{10} of $2.9 \text{ m}^3 \text{ m}^{-2}$ during the 2000-2017 period. FAC_{10} observations also indicated that meltwater may percolate deeper than 10 m from the surface making FAC_{10} insufficient to describe the retention capacity of the firn there. In a similar way, Machguth et al. (2016) showed that under conditions not completely understood, ice formation may prevent meltwater from accessing the entire top 10 m of firn. Therefore, further investigation of the firn permeability will help to understand how much of the FAC is used for meltwater retention. The firn area delineation and FAC_{10} dataset and maps can be used to constrain firn models and monitor the future evolution of the firn and are available for download at www.promice.dk.

5. Acknowledgement and data availability

This work is part of the Retain project funded by the Danish Council for Independent research (Grant no. 4002-00234) and the Programme for Monitoring of the Greenland Ice Sheet (www.PROMICE.dk). The FirnCover field campaigns were funded by the NASA grant NNX15AC62G. Achim Heilig was supported by DFG grant HE 7501/1-1. The source code is available at github.com/BaptisteVandecrux/FAC10_study. We thank Hubertus Fischer (Climate and Environmental Physics,



University of Bern) for providing low resolution density data from firn cores drilled during the EGIG expeditions 1990 and 1992.

5 6. References

- Ahlstrøm, A., Gravesen, P., Andersen, S., Van As, D., Citterio, M., Fausto, R., . . . Peters, D. &.: A new programme for monitoring the mass loss of the Greenland ice sheet, *Geol. Surv. Denmark Greenland Bull.*, 15, 61-64, 2008.
- Albert, M., and Shultz, E.: Snow and firn properties and air–snow transport processes at Summit, Greenland, *Atmos. Environ.*, 36, 2789-2797, 2002.
- 10 Alley, R.: Transformations in Polar Firn, Ph.D. Thesis, University of Wisconsin, Madison, WI, USA, 1987.
- Arthern, R. J., Vaughan, D. G., Rankin, A., Mulvaney, R., and Thomas, E. R.: In situ measurements of Antarctic snow compaction compared with predictions of models, *J. Geophys. Res.-Earth*, 115, F3, doi:10.1029/2009JF001306, 2010.
- Bader, H.: Sorge's law of densification of snow on high polar glaciers, *Journal of Glaciology*, 2, 15, 319-411, 1954.
- 15 Baker, I.: Density and permeability measurements with depth for the NEEM 2009S2 firn core, ACADIS Gateway, doi:10.18739/A2Q88G, 2012.
- Benson, C. S.: Stratigraphic Studies in the Snow and Firn of the Greenland Ice Sheet, U.S. Army Snow, Ice and Permafrost Research Establishment, 1962.
- Bolzan, J. F., and Strobel, M.: Oxygen isotope data from snowpit at GISP2 Site 15., PANGAEA, 20 doi:10.1594/PANGAEA.55511, 1999.



- Box, J.: Greenland ice sheet mass balance reconstruction. Part II: Surface mass balance (1840-2010), *J. Climate*, 26, 6974-6989, doi:10.1175/JCLI-D-12-00518.1, 2013.
- Box, J., Cressie, N., Bromwich, D. H., Jung, J.-H., Broeke, M. v., Angelen, J. V., . . . McConnell, J. R.: Greenland ice sheet mass balance reconstruction. Part I: Net snow accumulation (1600-2009), *J. Climate*, 26, 3919-3934, doi:10.1175/JCLI-D-12-00373.1, 2013.
- 5
- Buchardt, S. L., Clausen, H. B., Vinther, B. M., and Dahl-Jensen, D.: Investigating the past and recent delta 18O-accumulation relationship seen in Greenland ice cores, *Clim. Past*, 8, 6, 2053-2059, 2012.
- Charalampidis, C., Van As, D., Box, J. E., Van Den Broeke, M. R., Colgan, L. T., Doyle, S. H., . . . Smeets, C. J.: Changing surface-atmosphere energy exchange and refreezing capacity of the lower accumulation area, West Greenland, *Cryosphere*, 9, 6, 2163-2181, doi:10.5194/tc-9-2163-2015, 2015.
- 10
- Citterio, M., and Ahlstrøm, A. P.: The aerophotogrammetric map of Greenland ice masses, *Cryosphere, Brief Communication*, 7, 445-449, doi:10.5194/tc-7-445-2013, 2013.
- Clausen, H., Gundestrup, N. S., Johnsen, S. J., Binchadler, R., and Zwally, J.: Glaciological investigations in the Crete area, Central Greenland: a search for a new deep-drilling Site, *Ann. Glaciol.*, 10, 10-15, 1988.
- 15
- Colgan, W., Pedersen, A., Binder, D., Machguth, H., Abermann, J., and Jayred, M.: Initial field activities of the Camp Century Climate Monitoring Programme in Greenland. *Geological Survey of Denmark and Greenland Bulletin, Geol. Surv. Denmark Greenland Bull.*, 41, 75-78, 2018.
- de la Peña, S., Howat, I. M., Nienow, P. W., Broeke, M. R., Mosley-Thompson, E., Price, S. F., . . . Sole, A.: Changes in the firn structure of the western Greenland Ice Sheet caused by recent warming, *Cryosphere*, 9, 1203-1211, doi:10.5194/tc-9-1203-2015, 2015.
- 20



- Fausto, R. S and the PROMICE team: The Greenland ice sheet – snowline elevations at the end of the melt seasons from 2000 to 2017, *Geol. Surv. Denmark Greenland Bull.*, 41, 71-74, 2018.
- Fausto, R. S., Box, J. E., Vandecrux, B., van As, D., Steffen, K., MacFerrin, M., . . . Braithwaite, R. J.: A Snow Density Dataset for Improving Surface Boundary Conditions in Greenland Ice Sheet Firn Modeling, *Front. Earth Sci.*, 6, 51, doi:10.3389/feart.2018.00051, 2018.
- Fettweis, X., Box, J., Agosta, C., Amory, C., C., K., Lang, C., . . . Gallée, H.: Reconstructions of the 1900–2015 Greenland ice sheet surface mass balance using the regional climate MAR model, *Cryosphere*, 11, 2, 1015-1033, doi:doi:10.5194/tc-11-1015-2017, 2017.
- Fischer, H., Wagenbach, D., Laternser, M., and Haeberli, W.: Glacio-meteorological and isotopic studies along the EGIG line, central Greenland., *J. of Glaciol.*, 41, 139, 515-527, 1995.
- Forster, R. R., Box, J. E., van den Broeke, M. R., Miège, C., Burgess, E. W., Angelen, J. H., . . . McConnell, J. R.: Extensive liquid meltwater storage in firn within the Greenland ice sheet., *Nat. Geosci.*, 7, 95-19, doi:10.1038/NGEO2043, 2014.
- Graeter, K. A., Osterberg, E., Ferris, D. G., Hawley, R. L., Marshall, H. P., Lewis, G., . . . Birkel, S.: Ice Core Records of West Greenland Melt and Climate Forcing, *Geophys. Res. Lett.*, 45, 7, doi:10.1002/2017GL076641, 2018.
- Harper, J., Humphrey, N., Pfeffer, W. T., Brown, J., and Fettweis, X.: Greenland ice-sheet contribution to sea-level rise buffered by meltwater storage in firn, *Nature*, 491, 240-243, doi:doi:10.1038/nature11566, 2012.
- Hawley, R. L., Courville, Z. R., Kehrl, L., Lutz, E., Osteberg, E., Overly, T. B., and Wong, G.: Recent accumulation variability in northwest Greenland from ground-penetrating radar and shallow cores along the Greenland Inland Traverse, *J. Glaciol.*, 60, 220, 375-382, doi:10.3189/2014JoG13J141, 2014.



- Heilig, A., Eisen, O., MacFerrin, M., Tedesco, M., and Fettweis, X.: Seasonal monitoring of melt and accumulation within the deep percolation zone of the Greenland Ice Sheet and comparison with simulations of regional climate modeling, *Cryosphere*, 12, 1851-1866, doi:10.5194/tc-12-1851-2018, 2018.
- Herron, M., and Langway, C.: Firn Densification: an Empirical Model, *J. Glaciol.*, 25, 93, 373-385, doi:10.3189/S0022143000015239, 1980.
- Humphrey, N. F., Harper, J. T., and Pfeffer, W. T.: Thermal tracking of meltwater retention in Greenland's accumulation area, *J. Geophys. Res.*, 117, F01010, doi:10.1029/2011JF002083, 2012.
- Jezeq, K. C.: Surface Elevation and Velocity Changes on the South Central Greenland Ice Sheet: 1980-2011 - Data Summary. BPRC Technical Report No. 2012-01, Byrd Polar Research Center, The Ohio State University, Columbus, Ohio, 2012.
- Kameda, T., Narita, H., Shoji, H., Nishio, F., Fuji, Y., and Watanabe, O.: Melt features in ice cores from Site J, southern Greenland: some implication for summer climate since AD 1550, *Ann. Glaciol.*, 21, 51-58, 1995.
- Koenig, L. S., Miège, C., Forster, R. R., and Brucker, L.: Initial in situ measurements of perennial meltwater storage in the Greenland firn aquifer, *Geophys. Res. Lett.*, 41, 81-85, doi:10.1002/2013GL058083, 2014.
- Kovacs, A., Weeks, W. F., and Michitti, F.: Variation of Some Mechanical Properties of Polar Snow, Camp Century, Greenland, CRREL Res. Rpt. 276, 1969.
- Langen, P., Fausto, R. S., Vandecrux, B., Mottram, R., and Box, J.: Liquid Water Flow and Retention on the Greenland Ice Sheet in the Regional Climate Model HIRHAM5: Local and Large-Scale Impacts., *Front. Earth Sci.*, 4, 110, doi:doi: 10.3389/feart.2016.00110, 2017.
- Langway, C. C.: Stratigraphic analysis of a deep ice core from Greenland, CRREL Res. Rpt. 77, 1967.



- Ligtenberg, S. R., Kuipers Munneke, P., Noël, B. P., and . van den Broeke, M.: Improved simulation of the present-day Greenland firn layer (1960–2016), *Cryosphere*, doi:10.5194/tc-12-1643-2018, 2018.
- Lomonaco, R., Albert, M., and Baker, I.: Microstructural evolution of fine-grained layers through the firn column at Summit, Greenland, *J. Glaciol.*, 57, 204, 2011.
- 5 Lucas-Picher, P., Wulff-Nielsen, M., Christensen, J. H., Aðalgeirsdóttir, G., Mottram, R., and Simonsen, S.: Very high resolution in regional climate model simulations for Greenland: Identifying added value, *J. Geophys. Res.*, 117, D02108, doi:10.1029/2011JD016267, 2012.
- Machguth, H., MacFerrin, M., As, D. v., Box, J., Charalampidis, C., Colgan, W., . . . Mosley-Thompson, E.: Greenland meltwater storage in firn limited by near-surface ice formation, *Nature Clim. Change*, 6, 390-395,
10 doi:10.1038/NCLIMATE2899, 2016.
- Mayewski, P., and Whitlow, S.: 2016. Snow Pit and Ice Core Data from Southern Greenland, 1984, NSF Arctic Data Center. doi:10.5065/D6S180MH, 2016.
- Mayewski, P., and Whitlow S.: Snow Pit Data from Greenland Summit, 1989 to 1993. NSF Arctic Data Center. doi:10.5065/D6NP22KX, 2016.
- 15 Miège, C., Forster R.C., B. J., Burgess, E., McConnell, J., Pasteris, D., and Spikes, V. B.: Southeast Greenland high accumulation rates derived from firn cores and ground-penetrating radar, *Ann. Glaciol.*, 54, 63, 322-332, doi:10.3189/2013AoG63A358, 2013.
- Morris, E. M., and Wingham, D. J.: Densification of polar snow: Measurements, modeling and implication for altimetry, *J. Geophys. Res.-Earth*, doi:10.1002/2013JF002898, 2014.
20



- Mosley-Thompson, E., McConnell, J., Bales, R., Li, Z., Lin, P.-N., and Steffen, K.: Local to regional-scale variability of annual net accumulation on the Greenland ice sheet from PARCA cores, *J. Geophys. Res.*, 106, 33839–33851, doi:10.1029/2001JD900067, 2001.
- 5 Nghiem, S. V., Hall, D. K., Mote, T. L., Tedesco, M., Albert, M. R., Keegan, K., . . . Neumann, G.: The extreme melt across the Greenland ice sheet in 2012, *Geophys. Res. Lett.*, 39, L20502, doi:10.1029/2012GL053611, 2012.
- Nolin, A., and Payne, M. C.: Classification of glacier zones in western Greenland using albedo and surface roughness from the Multi-angle Imaging SpectroRadiometer (MISR), *Remote Sens. Environ.*, 107, 1-2, 264-275, doi:10.1016/j.rse.2006.11.004, 2007.
- Porter, S., and Mosley-Thompson, E.: Exploring seasonal accumulation bias in a west central Greenland ice core with
10 observed and reanalyzed data, *J. Glaciol.*, 60, 224, 1065-1074, doi:10.3189/2014JG13J233, 2014.
- Reed, S.: Performance Study of the Dewline Ice Cap Stations, 1963, CRREL Special Report 72, 1966.
- Reeh, N.: A nonsteady-state firn-densification model for the percolation zone of a glacier, *J. Geophys. Res.*, 113, F03023, doi:10.1029/2007JF000746, 2008.
- Renaud, A.: Etude physiques et chimiques sur la glace de l'indlandsis du Groenland , *Medd. Groenland*, 2, 177, 100-107,
15 1959.
- Spencer, M. K., Aller, R. B., and Creyts, T. T.: Preliminary firn-densification model with 38-site dataset, *J. Glaciol.*, 47, 159, 671-676, 2001.
- Steen-Larsen, H. C., Masson-Delmotte, V., Sjolte, J., Johnsen, S. J., Vinther, B. M., Bréon, F.-M., . . . : Understanding the climatic signal in the water stable isotope records from the NEEM cores, *J. Geophys. Res.*, 116, D06108, doi:10.1029/2010JD014311, 2011.
20



Steger, C., Reijmer, C., Broeke, M. v., Wever, N., Forster, R., Koenig, L., . . . Noël, B.: Firn meltwater retention on the Greenland ice sheet: a model comparison, *Front. Earth Sci.*, 5:3, doi:10.3389/feart.2017.00003, 2016.

5 Vallelonga, P., Christianson, K., Alley, R. B., Anandakrishnan, S., Christian, J. E., Dahl-Jensen, D., . . . Popp, T.: Initial results from geophysical surveys and shallow coring of the Northeast Greenland Ice Stream (NEGIS), *Cryosphere*, 8, 1275-1287, doi:10.5194/tc-8-1275-2014, 2014.

van den Broeke, M. R., Enderlin, E. M., Howat, I. M., Kuipers Munneke, P., Noël, B. P., van de Berg, W. J., . . . Wouters, B.: On the recent contribution of the Greenland ice sheet to sea level change, *Cryosphere*, 10, 1933-1046, doi:doi:10.5194/tc-10-1933-2016, 2016.

10 van der Veen, C. J., Mosley-Thompson, E., Jezek, K. C., Whillans, I. M., and Bolzan, J. F.: Accumulation rates in South and Central Greenland, *Polar Geography*, 25, 2, 79-162, doi:10.1080/10889370109377709, 2001.

Wilhelms, F.: Measuring the Conductivity and Density of Ice Cores, *Ber. Polarforsch.*, 191, 1996.

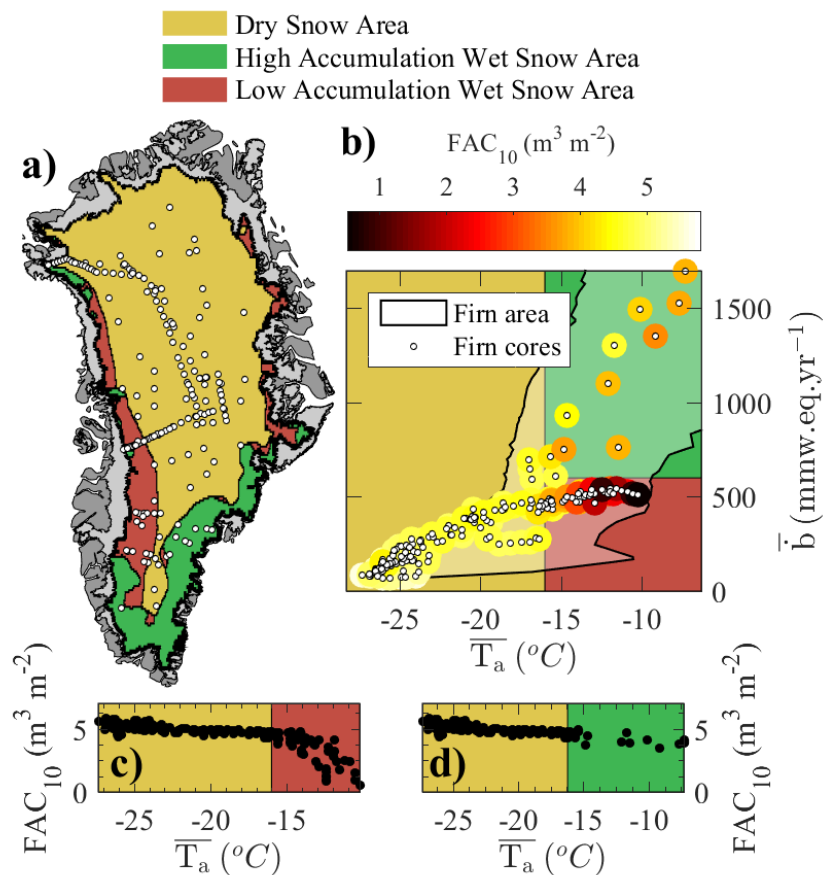


Figure 1. a) Geographical distribution of the FAC₁₀ dataset. b) Distribution of the dataset in the accumulation-temperature space (\bar{b} and \bar{T}_a). FAC₁₀ value is indicated by a coloured disk around each point. c) Temperature dependency of FAC₁₀ in the DSA and LAWSA d) Temperature dependency of FAC₁₀ in the DSA and HAWSA.

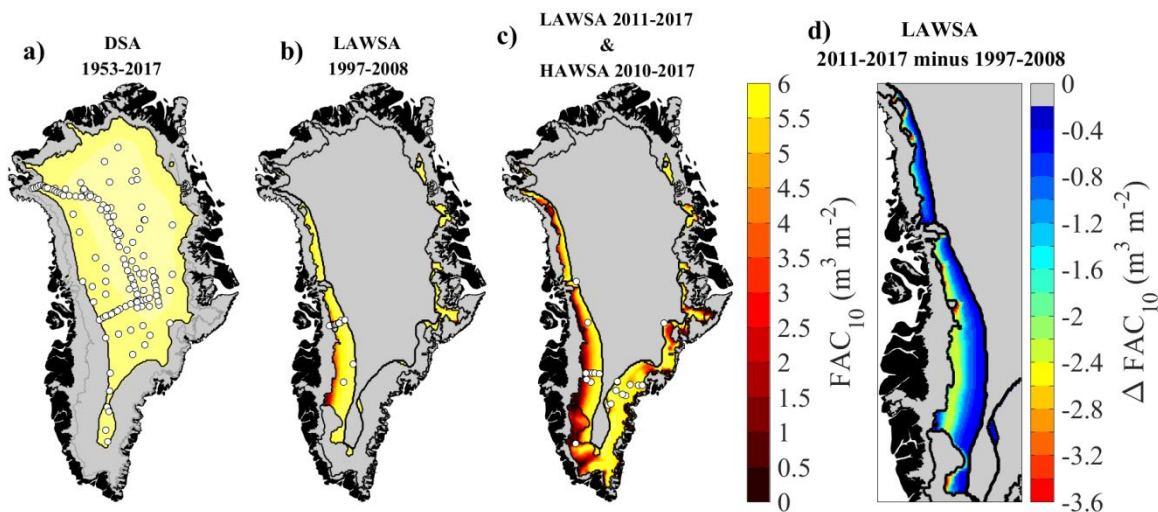
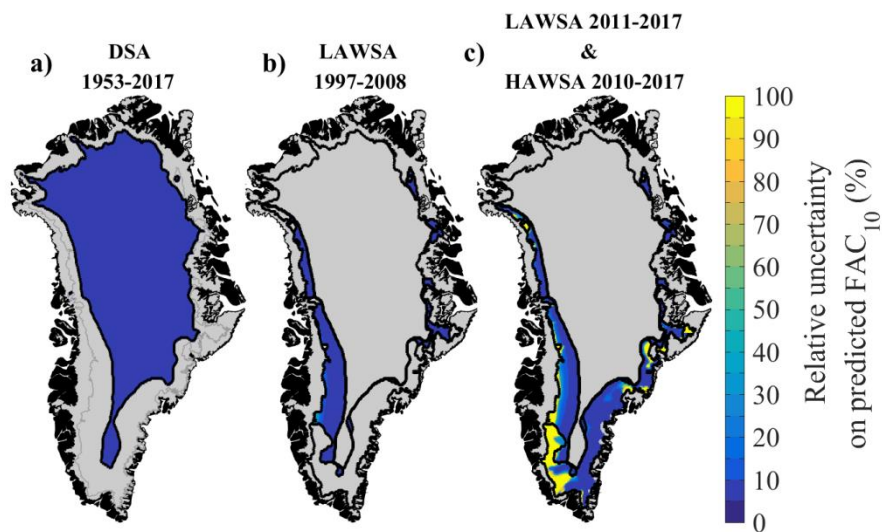


Figure 2. FAC_{10} maps and location of the FAC_{10} measurements (a, b, c). Map of the change in FAC_{10} between the 1997-2008 and 2011-2017 periods in the LAWSA (c).



5 Figure 3. Maps of the relative uncertainty of the FAC_{10} maps in the DSA (a), LAWSA for the 1997-2008 period (b) and in the LAWSA for 2011-2017 and in the HAWSA for 2010-2017 period (c).



Table 1. List of the publications presenting the firn cores used in this study.

Source	Number of cores	Source	Number of cores
Albert and Shultz (2002)	1	Langway (1967)	1
Alley (1987)	1	Lomonaco et al. (2011)	1
Bader (1954)	1	Machguth et al. (2016)	28
Baker (2012)	1	Mayewski and Whitlow (2016a)	1
Benson (1962)	55	Mayewski and Whitlow (2016b)	1
Bolzan and Strobel (1999)	9	Miège et al. (2013)	3
Buchardt et al. (2012)	8	Morris and Wingham (2014)	66
Clausen et al. (1988)	8	Mosley-Thompson et al. (2001)	31
Colgan et al. (2018)	1	Porter and Mosley-Thompson (2014)	1
Fischer et al., (1995)	14	Reed (1966)	1
Forster et al. (2014)	5	Renaud (1959)	7
Hawley et al. (2014)	8	Spencer, et al. (2001)	8
Harper et al. (2012)	32	Steen-Larsen et al. (2011)	1
Jezek (2012)	1	Vallelonga et al. (2014)	1
Kameda et al. (1995)	1	van der Veen et al. (2001)	10
Koenig et al. (2014)	3	Wilhelms (1996)	13
Kovacs et al. (1969)	1	This study	20